Scattering from long prisms computed using ray tracing combined with diffraction on facets

Evelyn Hesse[*], Zbigniew Ulanowski

Department of Physical Sciences, University of Hertfordshire, Hatfield, AL10 9AB, UK.

Abstract

A new model suitable for rapid computation of scattering on faceted dielectric objects such as ice crystals is presented. It combines ray tracing with diffraction on flat facets. The model allows retaining the ray nature of the internal field by calculating the diffraction component using an approximation for the far field direction of the Poynting vector. While this approach is similar to methods using the uncertainty principle, it does not require the use of angular distributions of diffracted rays, which leads to negligible computational overheads with respect to pure ray tracing. Results showing angle-dependent scattering computed for long hexagonal prisms, including phase functions and degree of linear polarization, are presented and compared with other models and with measurements on hexagonal fibers.

Keywords: light scattering; diffraction; ice crystals; cirrus

1. Introduction

The significance of ice and mixed-phase clouds to the earth-atmosphere radiation balance and climate is well established. Yet, present understanding of cirrus with regard to scattering properties of ice crystals is weak, which is mainly due to inadequate theoretical models. For realistic crystal shapes and sizes accurate models either do not exist, have not yet been adequately verified or are computationally very demanding, especially for larger size parameters. A modified Kirchhoff approximation (MKA) method has been introduced [1] to calculate far fields from classical geometric optics (GO) results, which encouraged the development of the improved GO model [2]. The latter is however computationally expensive. For moderate values of the size parameter the finite difference time domain (FDTD) method can be used [3] but it puts even more severe demands on computational resources. Thus, despite its limitations, geometric optics (GO) combined with projected-area diffraction [4] is still the most widely used model for moderate to large size parameters. Therefore, substantial improvement in the theory of scattering on ice crystals is important if phenomena such as radiative forcing by cirrus are to be understood and the sign and magnitude of cirrus cloud-climate feedback established.

We are proposing a method using an approximation for the far field direction of the Poynting vector to modify ray tracing calculations of scattering on faceted dielectric bodies to take into account the diffraction of light refracted by and reflected from the facets. This approach has similarities with methods using the uncertainty principle to include diffraction in ray tracing calculations, particularly for modeling stray light in optical systems, which were incorporated into commercial software [5-9]. The authors of these papers use a particle

[*] *Corresponding author. Tel: +44 1707 286363, fax: +44 1707 284644.*

E-mail address: e.hesse@herts.ac.uk

approach, assuming the uncertainty in the direction of propagation of a photon to be proportional to its distance from the edge of an aperture. Consequently, diffraction is modeled as generation of a ray bundle normally distributed in angle and with a width inversely proportional to the distance of the ray from the edge.

In our method the Monte Carlo traces represent approximations of energy flow lines rather than single photon rays. Diffraction deflects the traces towards the nearest edge. Diffraction theory shows that the extent to which a wave is diffracted increases with decreasing aperture size to wavelength ratio. In a similar fashion, the bending of energy flow lines increases with decreasing distance to a sharp edge for diffraction by a half-plane [10,11].

In the following, the far field deflection of energy flow lines and the angular intensity distribution of light diffracted by a half plane, as obtained from exact theory [10], are compared with analytical expressions. We then modify these expressions in order to describe diffraction on a slit and compare the results with the Fraunhofer diffraction pattern. Finally, light scattering on long hexagonal columns in the case of perpendicular incidence is investigated. The derived expressions are used to account for the diffraction occurring simultaneously with reflection and refraction on crystal facets, and the results are compared with theoretical models and experiments.

2. Computational Methods
2.1. Diffraction by a half-plane

Rigorous diffraction theory provides comparatively simple solutions for diffraction of a plane wave by a half plane. Therefore, this system is used here to study field distributions and energy flow of a diffracted wave [10,11]. We consider a perfectly conducting half-plane placed in Cartesian coordinates at $y=0$, $x>0$. In the case of E-polarization the incident electric field vector is assumed to be parallel to the edge of the half plane (Fig. 1) and its components can be specified as $E_x^{(i)}=E_y^{(i)}=0$ and

$$E_z^{(i)} = \sqrt{\frac{2}{\varepsilon_0}} e^{-ikr\cos(\theta-\alpha_0)} \tag{1}$$

where r and θ are polar coordinates related to x and y by the equations $x=r\cos(\theta)$, $y=r\sin(\theta)$, α_0 is the angle between the positive x-axis and the direction of propagation, k and ε_0 are the wave number and vacuum permittivity, respectively.
The complete field can be written in the form

$$E_z = \sqrt{\frac{2}{\pi\varepsilon_0}} e^{-\frac{1}{4}i\pi} \left\{ e^{-ikr\cos(\theta-\alpha_0)} F[-\sqrt{2kr}\cos\frac{1}{2}(\theta-\alpha_0)] - e^{-ikr\cos(\theta+\alpha_0)} F[-\sqrt{2kr}\cos\frac{1}{2}(\theta+\alpha_0)] \right\} \tag{2}$$

where $F[a] = \int_a^\infty e^{i\xi^2} d\xi$ is the complex Fresnel integral. The polar angle θ has to be represented by a value $0 \le \theta < 2\pi$.
With a time factor exp($-i\omega t$) suppressed the 2nd Maxwell's equation in free space is

$$\nabla \times \bar{E} = i\sqrt{\frac{\mu_0}{\varepsilon_0}} k\bar{H} \tag{3}$$

where μ_0 is the vacuum permeability.
Equating to zero all partial derivatives with respect to z, this may be split up into

$$H_x = \frac{1}{ik}\sqrt{\frac{\varepsilon_0}{\mu_0}} \frac{\partial E_z}{\partial y}, \quad H_y = -\frac{1}{ik}\sqrt{\frac{\varepsilon_0}{\mu_0}} \frac{\partial E_z}{\partial x} \tag{4}$$

The time-averaged Poynting vector is given by

$$\langle \bar{S} \rangle = \frac{1}{2}\Re(\bar{E} \times \bar{H}^*) = \frac{1}{2}\Re(-E_z H_y^*, E_z H_x^*, 0) \tag{5}$$

In the case of H-polarization, when the incident field is specified by $H_x^{(i)}=H_y^{(i)}= 0$ and

$$H_z^{(i)} = \sqrt{\frac{2}{\mu_0}} e^{-ikr\cos(\theta-\alpha_0)} \tag{6}$$

the complete field is given by

$$H_z = \sqrt{\frac{2}{\pi\mu_0}} e^{-\frac{1}{4}i\pi} \left\{ e^{-ikr\cos(\theta-\alpha_0)} F[-\sqrt{2kr}\cos\frac{1}{2}(\theta-\alpha_0)] + e^{-ikr\cos(\theta+\alpha_0)} F[-\sqrt{2kr}\cos\frac{1}{2}(\theta+\alpha_0)] \right\} \tag{7}$$

With a time factor exp(-$i\omega t$) suppressed the 1st Maxwell's equation in free space is

$$\nabla \times \bar{\mathbf{H}} = -i\sqrt{\frac{\varepsilon_0}{\mu_0}} k\bar{\mathbf{E}} \tag{8}$$

Equating to zero all partial derivatives with respect to z, this may be split up into

$$E_x = -\frac{1}{ik}\sqrt{\frac{\mu_0}{\varepsilon_0}}\frac{\partial H_z}{\partial y} \quad , \quad E_y = \frac{1}{ik}\sqrt{\frac{\mu_0}{\varepsilon_0}}\frac{\partial H_z}{\partial x} \tag{9}$$

The time-averaged Poynting vector is now given by

$$\langle\bar{\mathbf{S}}\rangle = \frac{1}{2}\Re(\bar{\mathbf{E}}\times\bar{\mathbf{H}}^*) = \frac{1}{2}\Re(E_y H_z^*, -E_x H_z^*, 0) \tag{10}$$

The energy flow lines can be obtained by solving the differential equation:

$$\frac{\mathrm{d}x}{\mathrm{d}y} = \frac{\langle S(x(y),y)\rangle_x}{\langle S(x(y),y)\rangle_y} \tag{11}$$

Energy flow lines for light incident perpendicularly to the half plane, i.e. $\alpha_0 = \pi/2$, calculated using eq. (11) for starting points at $y=0$ are shown in Fig. 2. It is immediately apparent that the closer to the edge the lines pass, the more strongly they are deflected in the far field and the shorter is the path until they approach their final direction.

Fig. 3 shows the far field deflection angle, defined as $\varphi = \theta - 3\pi/2$, of energy flow lines for unpolarized light calculated using eq. (11) for $\alpha_0 = \pi/2$ and plotted as a function of $-x/\lambda$, where $-x$ is the distance to the edge at which the lines pass the half-plane. It can be seen that the far field deflection angle decreases monotonically over the investigated range of x. For $-x/\lambda \to 0$ or ∞ it approaches $\pi/2$ or 0, respectively. The function

$$\varphi(x) = \arctan(\lambda/(4\pi^2 x)) \tag{12}$$

is a good fit to the numerically calculated values of the deflection angle.

The function $(\mathrm{d}\varphi/\mathrm{d}x)^{-1}(\varphi)$ is proportional to an angular energy density $w(\varphi)$ in the far field:

$$w(\varphi) = -\left(\frac{\mathrm{d}\varphi}{\mathrm{d}x}\right)^{-1}\left[\frac{\mathrm{d}W}{\mathrm{d}x}\right]^{(i)}$$

For homogeneous illumination the linear energy density of the field incident at the half plane $[\mathrm{d}W/\mathrm{d}x]^{(i)}$ is a constant, which will be set to unity. Fig. 4 shows $-(\mathrm{d}\varphi/\mathrm{d}x)^{-1}$ plotted against φ for both the far field deflection angle calculated from rigorous diffraction theory, as represented by eq. (10) and (11), and from the analytic function (12). For the latter one we obtain after replacing x by $\lambda/(4\pi^2\tan\varphi)$:

$$w(\varphi) = -\left(\frac{\mathrm{d}\varphi}{\mathrm{d}x}\right)^{-1} = -\left(\frac{\mathrm{d}\arctan(\lambda/(4\pi^2 x))}{\mathrm{d}x}\right)^{-1} = \frac{\lambda}{4\pi^2\sin^2\varphi} \tag{13}$$

The two graphs can be seen to agree reasonably well.

We now show that eq. (13) can be derived directly by considering asymptotic variants of the rigorous diffraction theory. For the far shadow region eq. (2) can be simplified, and the following approximate expression is obtained for the E-polarization field [10]:

$$E_z = \frac{2}{\sqrt{\pi\varepsilon_0}} e^{\frac{1}{4}i\pi} \frac{\sin\frac{\alpha_0}{2}\sin\frac{\theta}{2}}{(\cos\alpha_0 + \cos\theta)} \frac{e^{ikr}}{\sqrt{kr}} \tag{14}$$

Using the identities

$$\langle w_e\rangle = \frac{1}{4}\bar{\mathbf{E}}\cdot\bar{\mathbf{D}}^* \, , \, D_z = \varepsilon_0 E_z \tag{15}$$

the time averaged energy density of the electric field can then be written as:

$$\langle w_e \rangle = \frac{1}{\pi k r} \frac{\sin^2 \frac{\alpha_0}{2} \sin^2 \frac{\theta}{2}}{(\cos \alpha_0 + \cos \theta)^2} \tag{16}$$

In the far field the wave will be approximately a plane one so that we can assume that the time averaged densities of the electric and magnetic fields are approximately equal:
$\langle w_m \rangle \approx \langle w_e \rangle$.

Therefore, the averaged energy density of the E-polarization field $\langle w \rangle_E \approx 2 \langle w_e \rangle$.

In a similar way, the following expression for the H-polarization field is obtained [10]:

$$H_z = -\frac{2}{\sqrt{\mu_0 \pi}} e^{\frac{1}{4} i \pi} \frac{\cos \frac{\alpha_0}{2} \cos \frac{\theta}{2}}{(\cos \alpha_0 + \cos \theta)} \frac{e^{ikr}}{\sqrt{kr}} \tag{17}$$

Considering again the far field angular distribution and using the expressions

$$\langle w_m \rangle = \frac{1}{4} \vec{B} \cdot \vec{H}^*, \quad B_z = \mu_0 H_z \tag{18}$$

we find that the averaged energy density of the magnetic field is

$$\langle w_m \rangle = \frac{1}{\pi k r} \frac{\cos^2 \frac{\alpha_0}{2} \cos^2 \frac{\theta}{2}}{(\cos \alpha_0 + \cos \theta)^2} \approx \langle w \rangle_H / 2 \tag{19}$$

where $<w>_H$ is the time averaged energy density of the H-polarized field.
For unpolarized light we have
$$\langle w \rangle = (\langle w \rangle_E + \langle w \rangle_H)/2 = \langle w_e \rangle + \langle w_m \rangle \tag{20}$$
In the case of perpendicular incidence ($\alpha = \pi/2$) we therefore obtain
$$\langle w \rangle = \frac{1}{2\pi k r \cos^2 \theta} \tag{21}$$
By omitting the radial dependence we obtain an equation for the angular energy density
$$\langle w(\varphi) \rangle \approx \frac{\lambda}{4\pi^2 \sin^2 \varphi} \tag{22}$$
which is identical to eq. (13).

2.2. Diffraction by a slit

In the previous section we have demonstrated that eq. (12) is a good approximation for far field deflection angles of energy flow lines, given as a function of the distance from the edge at which the lines pass the half-plane. Here we extend this approach to diffraction on a slit. For this purpose we modify eq. (12) as follows:

$$\varphi(x) = \arctan\left(\frac{\lambda}{4\pi^2} \left(\frac{1}{x} - \frac{1}{2a - x} \right) \right) \tag{23}$$

where $2a$ is the width of the slit. This equation gives zero deflection for $x=a$ (middle position in the slit), and for positions close to the edges ($x \to 0$, $x \to 2a$) it reduces to the equation for a half-plane.
Using this expression, the following far field angular energy distribution is obtained:

$$\langle w(\varphi) \rangle = -\left(\frac{\partial \varphi}{\partial x} \right)^{-1} = \frac{(4\pi)^2 + \left(\frac{1}{x} - \frac{1}{2a - x} \right)^2}{4\lambda \left(\frac{1}{x^2} + \frac{1}{(2a - x)^2} \right)} \tag{24}$$

In eq. (24) x can be substituted by the following expression obtained by solving eq. (23) for x:

$$x = \frac{4\pi^2 a \tan(\varphi) + \lambda - \sqrt{16\tan^2(\varphi)\pi^4 a^2 + \lambda^2}}{4\pi^2 \tan(\varphi)}$$

Eq. (24) now becomes

$$\langle w(\varphi) \rangle = \frac{\lambda}{2\pi^2 \sin^2(\varphi)} \frac{(F+1)/2 - \sqrt{F}}{F - \sqrt{F}} \tag{25}$$

where $F = \left(4\pi^2 a \tan(\varphi)/\lambda\right)^2 + 1$.

One should note that for $\varphi \rightarrow \pm\pi/2$, which corresponds to a small passing distance from one of the two facet edges, eq. (25) becomes identical to eq. (13) for diffraction on a half plane. Fig. 5 shows the familiar Fraunhofer diffraction pattern for $a/\lambda=5$ together with the result of eq. (25). Apart from the fact that eq. (25) does not take interference into account, a good general agreement with the Fraunhofer diffraction pattern is found.

To model scattering on long prisms, such as hexagonal columns, eq. (23) was implemented into a geometric optics ray tracing code [4]. In this implementation both, reflected and refracted rays are bent towards the nearest edge of a facet by an angle obtained from eq. (23). At present the implementation is essentially 2-dimensional: it applies to infinitely long prisms at normal incidence. External diffraction, which is implemented in the ray tracing code [4] by Fraunhofer diffraction on the projected cross section of the object, was retained except that the circular aperture was replaced by a slit.

3. Results
3.1. Scattering – comparison with other models

The new model was compared with GO calculations enhanced by external diffraction [4] (in the following called classical GO), and computations using an analytical technique, the separation of variables method (SVM) [12,13]. Fig. 6 shows phase functions and degree of linear polarization for an axially randomized hexagonal column ($n=1.31$, size parameters 50 and 100) at normal incidence obtained using these three methods. The phase function is much improved in the halo region compared to the sawtooth like shape in classical GO. Additionally, the phase function shows a strong improvement in the backscattering region, where classical GO predicts a sharply confined high angular intensity region between 142° and 162°. The absolute linear polarization in most of the backscattering region is reduced. The results obtained with the new model are slightly closer to SVM results for size parameter 100 than for 50. Due to the applied far field approximation of deflection angles and the fact that phase tracing is not included in the current version of the model a decrease in accuracy for very low size parameters is expected.

3.2 Scattering - experimental comparison

SVM calculations are practicable for size-parameters up to approximately 100 [13]. For larger size parameters the model can be tested using experimental results. The authors have recently developed new ice crystal analogues, which are suitable for use at optical wavelengths. Of these, long, thin, hexagonal glass fibres [14,15] are convenient for the testing of theoretical models for infinite cylinders such as the one described here. Scattering measurements were carried out using a fibre optics diffractometer covering the range of scattering angles between 3 and 177° [16]. An air-cooled Ar-ion laser was the light source. A dual-wavelength quarter-wave plate was used to produce circular polarization, and a prism to select the 514.5 nm emission line of the laser. The fibres were mounted on a two-axis goniometric cradle attached to a motorized rotation stage. The fibre axis was set normal to the scattering plane. Fig. 7 shows the phase function measured for a hexagonal glass fiber ($n=1.7407$, diameter 25 µm corresponds to size parameter 153) in air, axially averaged over 360° with a 5 degree increment. This discrete averaging accounts for the presence of peaks spaced at 10° intervals in the 70° to 180° region; these peaks are due to external reflection. Experimental and calculated phase functions agree well, with some improvement over the classical GO model near the halo peak (located at 61° for n=1.7407).

4. Discussion

A new model suitable for rapid computation of scattering on faceted dielectric objects has been developed. It combines ray tracing with diffraction on flat facets. The model allows retaining the ray nature of the internal field by calculating the diffraction component using an approximation for the far field direction of the Poynting vector. The angle of diffraction of a ray transmitted through or reflected from a facet is calculated from the ray's proximity to the facet edges. While this approach is similar to methods utilizing the uncertainty principle [5-9], the model does not require the use of angular distributions of diffracted rays, respectively, at each ray interaction or external reflection and outward refraction, which leads to negligible computational overheads in comparison with pure GO. For diffraction by a half-plane the result is analytically identical to the unpolarized light, large angle asymptotic solution of the exact diffraction theory due to Sommerfeld [10]. A further advantage of the model over pure GO is that it avoids the difficulty posed by directly transmitted rays (δ-rays), as essentially all rays are diffracted to a greater or lesser extent. The model can be extended to 3-dimensional objects.

In the context of scattering on ice crystals, the new model is particularly suitable for visible wavelengths where ice is weakly absorbing and multiple internal reflections contribute strongly to scattering. A comparison with classical GO and exact SVM (Fig. 6) reveals that the new model produces phase functions substantially nearer to the SVM results than does classical GO. One notable feature of the phase functions calculated using the new model is the broadening of the 22° halo peak observed for lower size parameters (see Fig. 6), an effect which GO alone does not predict as it is essentially size independent. This broadening offers one possible explanation for the fact that halos are rarely produced by cirrus clouds (the other one being that smooth, column-like crystals are rarely found in cirrus).

While similar results can be obtained using MKA [1], the improved GO model [2] or for smaller size parameters the FDTD method [3] and, so far for columns, the T-matrix method, [17] these approaches are computationally very demanding and are not yet available to the broader community of atmospheric researchers. Consequently, GO combined with projected-area diffraction is still the most widely used model for moderate to large size parameters, notwithstanding its severe limitations. The new model has a significant advantage over existing GO codes, as it is their natural, straightforward extension but does not add a significant computational overhead, despite being more accurate. The model can be further improved, e.g. by tracing phase as well as amplitude of a "ray" (although this should not be important for scattering of natural, i.e. incoherent light), including deviations from far field diffraction for small size parameters, and by introducing external diffraction of rays passing close to an edge after leaving the crystal. Since the model is, in principle, applicable to crystals of arbitrary complexity and can be used for large crystals, it promises to fill a substantial niche in the shape/size parameter space for scattering at solar wavelengths.

Acknowledgement

References

[1]   Muinonen K. Scattering of light by crystals: a modified Kirchhoff approximation. Appl. Opt. 1989;28:3044.

[2]   Yang P, Liou KN. Geometric-optics-integral equation method for light scattering by nonspherical ice crystals. Appl. Opt. 1996;35:6568.

[3]   Yang P, Liou KN. In: Mishchenko MI, Hovenier JW, Travis LD, editors. Light scattering by nonspherical particles. New York: Academic Press, 1999. p.173-221.

[4]   Macke A, Mueller J, Raschke E. Single scattering properties of atmospheric ice crystals. J. Atmos. Sci. 1996;53:2813.

[5]   Carlin P. The minimum spot size for a focused laser and the uncertainty relation. Proc. IEEE 1964;52:1371.

[6]   Coffey KL. Next-Generation Earth Radiation Budget Instrument Concepts. Thesis (Virginia Tech, Blacksburg, 1998). http://scholar.lib.vt.edu/theses/

[7]   Heinisch RP, Chou TS. Numerical experiments in modeling diffraction phenomena. Appl. Opt. 1971;10:2248.

[8]   Likeness BK. Stray light simulations with advanced Monte Carlo techniques. Proc. SPIE 1977;107:80.

[9]   Freniere ER, Gregory, GG, and Hassler, RA. Edge diffraction in Monte Carlo ray tracing. Proc. SPIE 1999;3780:151.

[10]   Born M, Wolf E. Principles of Optics. 7th ed. (CUP, Cambridge, 1999).

[11]   Braunbek W, Laukien G. Einzelheiten zur Halbebenen-Beugung. Optik 1952;9:174.

[12]   Havemann S, Rother T, Schmidt K. Light scattering by hexagonal ice crystals. Conf. on Light Scattering by Nonspherical Particles: Theory, Measurements and Applications. 29th Sept.-1st Oct. 1998, New York. Am. Meteorol. Soc., Ed. Mishchenko MI, Travis LD and Hovenier JW. p. 253-56.

[13]   Rother, T, Schmidt, K, Havemann, S. Light scattering on hexagonal ice columns. J. Opt. Soc. Am. A 2001;18:2512.

[14]   Ulanowski Z, Hesse E, Kaye PH, Baran AJ, Chandrasekhar R, Parfitt C. Scattering of light from ice crystal analogues. Proc. 6th Int. Congr. Optical Particle Charact., Brighton 2001, p. 81-82.

[15]   Ulanowski Z, Hesse E, Kaye PH, Baran AJ, Chandrasekhar R. Scattering of light from atmospheric ice analogues. JQSRT (submitted, this issue).

[16]   Ulanowski Z, Greenaway RS, Kaye PH, Ludlow IK. Laser diffractometer for single particle scattering measurements. Measurement Sci. Technol. 2002;13:292.

[17]   Havemann S, Baran AJ. Extension of T-matrix to scattering of electromagnetic plane waves by non-axisymmetric dielectric particles. JQSRT 2001;70:139.
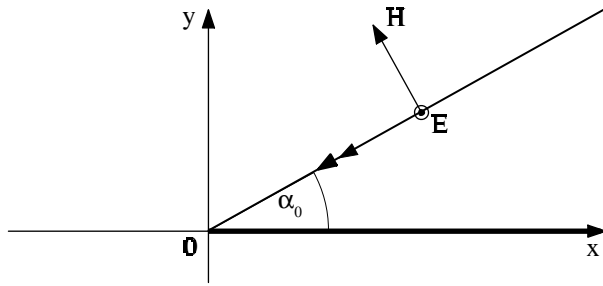
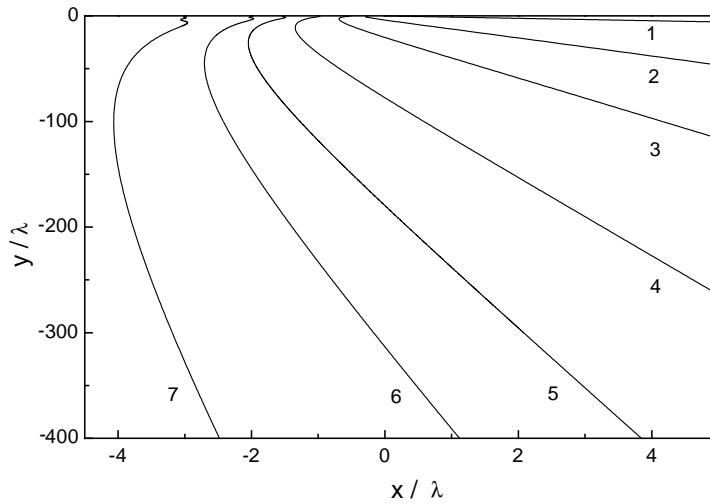Fig. 1. *E*-polarized plane wave incident on a perfectly conducting half-plane.

Fig. 2. Time averaged energy flow lines for perpendicular incidence on a half plane positioned at *x*=0, *y*>0. The distance in wavelengths from the edge at *y*=0 for graphs 1 to 7 is 0.025, 0.25, 0.5, 1.0, 1.5, 2.0 and 3.0, respectively.
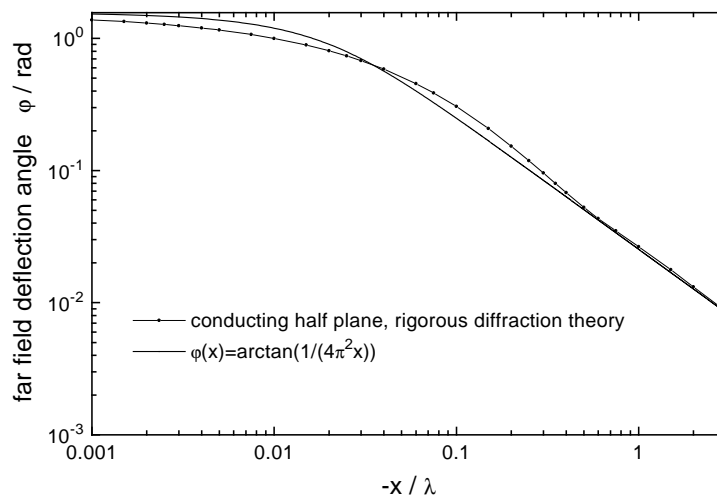

Fig. 3. Far field deflection angle of energy flow lines of unpolarized light as a function of –*x*/λ, where *x* is the distance to the edge at which the lines pass the half-plane, calculated using eq. (11).

8
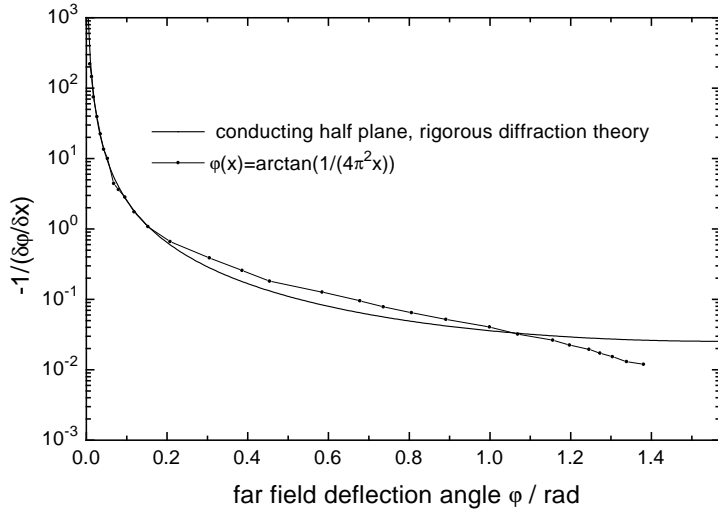
Fig. 4. The functions $(-\mathrm{d}\varphi/\mathrm{d}x)^{-1}$ plotted against φ for both the far field deflection angle calculated using rigorous diffraction theory, and for the analytic function (12).
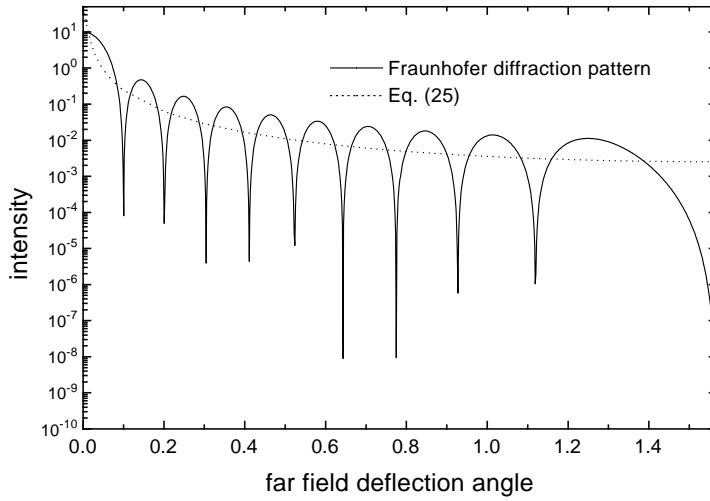

Fig. 5. Angular intensity distribution for diffraction on a slit ($a/\lambda=5$): Fraunhofer diffraction pattern and analytical function $\varphi(x) = \arctan\left[\dfrac{\lambda}{4\pi^2}\left(\dfrac{1}{x} - \dfrac{1}{2a-x}\right)\right]$.
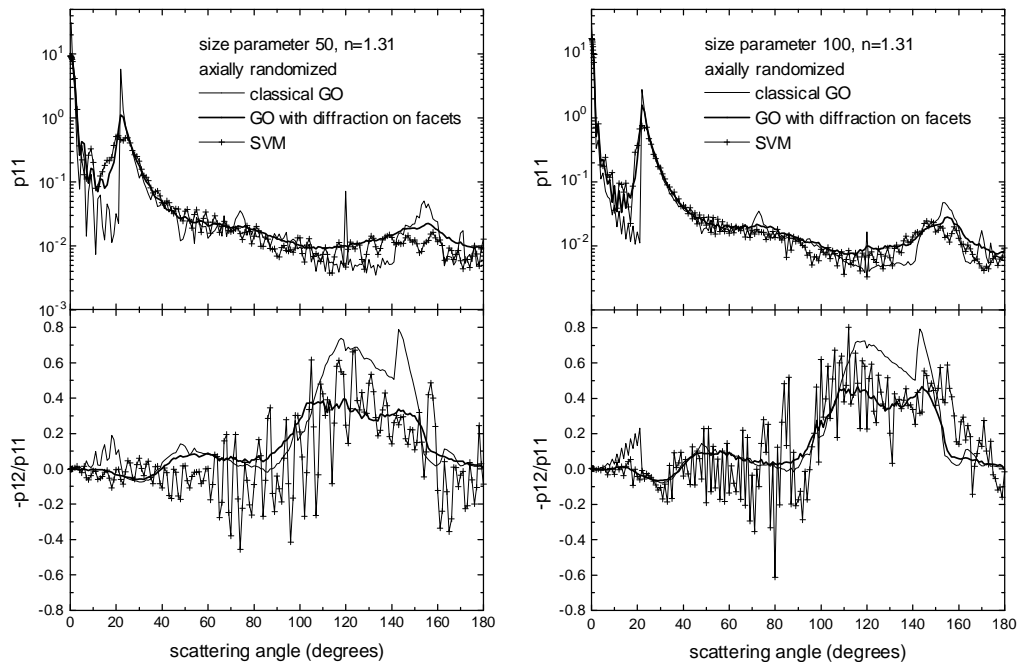
Fig. 6. Phase function and degree of linear polarization for an axially randomized hexagonal column with a refractive index of 1.31 and size parameters 50 and 100, respectively, at normal incidence, calculated using the new model in comparison with classical GO [4] and SVM [12] computations.
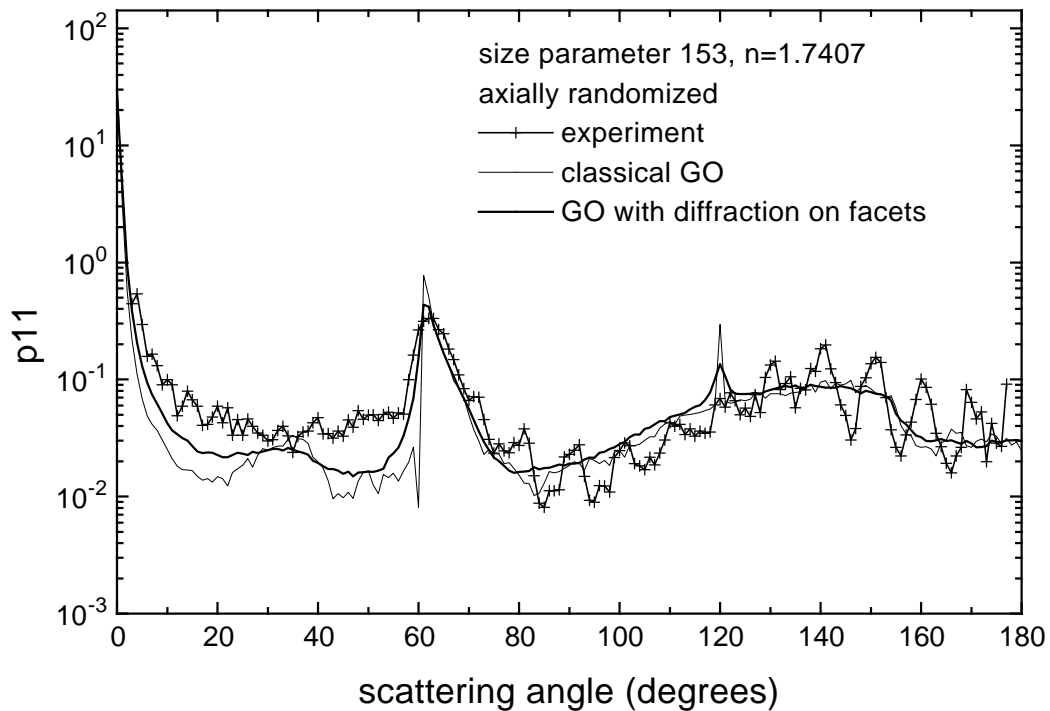

Fig. 7. Phase function for axially randomized hexagonal column with a size parameter 153 and refractive index of 1.7407, at normal incidence, experimental result and calculation using the new model in comparison with classical GO [4].